	Entropy: II				
Saeki K, Yasugi E, Okuma E, Breit SN, Nakamura M, Toda T, Kaburagi Y, Yuo A	Proteomic analysis on insulin signaling in human hematopoietic cells: identification of CLIC1 and SRp20 as novel downstream effectors of insulin.	Am J Physiol Endocrinol Metab	289	419-428	2005
Omi K, Kuriyama K, Yamada K, Oku H, Kano S, Sato K, Suzuki H, Katakai R	Synthetic study of an antigenic peptide having a partial sequence from Plasmodium falciparum enolase.	Peptide Science		637-640	2005
Yamamoto EC, Mizuno M, Nishikawa K, Miyazawa S, Zhang L, Matsuo S, Natori Y	Shiga toxin-1 causes direct renal injury in rats.	Infect Immun	73	7099-7106	2005
Osawa E, Nakajima A, Fujisawa T, Kawamura YI, Toyama-Sorimachi N, Nakagama H, Dohi T.	Predominant T Helper Type 2-Inflammatory Responses Promote Murine Colon Cancers.	Int J Cancer	In press		2005
Kanai T, Kawamura T, Dohi T, Makita S, Nemoto Y, Totsuka T, Watanabe M.	TH1/TH2-Mediated Colitis Induced by Adoptive Transfer of CD4+CD45RBhigh T Lymphocytes Into Nude Mice.	Inflamm Bowel Dis	12	89	2006
Dohi T, Ejima C, Kato R, Kawamura YI, Kawashima R, Mizutani N, Tabuchi Y, Kojima I.	Therapeutic potential of follistatin for colonic inflammation in mice.	Gastroenterology	128	411	2005
Y. Hamano, K. Tsukamoto, M. Abe, G.D. Sun, D. Zhang, H. Fujii, S. Matsuoka, M. Tanaka, A. Ishida-Okawara, H. Tachikawa, H. Nishimura, K. Tokunaka, O. Hino, S. Hirose, and K. Suzuki.	Genetic Dissection of Vasculitis, Myeloperoxidase-Specific Antineutrophil Cytoplasmic Antibody Production, and Related Traits in Spontaneous Crescentic Glomerulonephritis-Forming/ Kinjoh Mice.	J. Immuno	In press		2006

W. Yumura, M. Itabashi, A. Ishida-Okawara, K. Tomizawa, J. Yamashita, Y. Kaneshiro, H. Nihei, and K. Suzuki.	A Novel Mouse Model for MPO-ANCA-Associated Glomerulonephritis.	Microbiol.Immunol.	In press		2006
N. Nagai-Miura, T. Harada, H. Shinohara, K. Kurihara, Y. Adachi, A. Ishida-Okawara, T. Oharaseki, K. Takahashi, S., Naoe, K. Suzuki and N. Ohno.	Lethal and severe coronary arteritis in DBA/2 mice induced by fungal pathogen, CAWS.	Atherosclerosis	In press		2006
A. S. Persad, Y. Kameoka, S. Kanda, Y. Niho, K. Suzuki.	Arginine to Cysteine Mutation (R499C) Found in a Japanese Patient with Complete Myeloperoxidase Deficiency.	Gene Expression	In press		2006
H. Yasuda, N. Yoshizawa, K. Suzuki	Modeling on social spread from immunity.	Jpn J Infect Dis	58	14-15	2005
K. Suzuki, K. Yamamoto and H. Yoshikura.	Focusing on Assessment of Risk to Communities in International Symposium on Infectious Agent Transmission Model Building.	Jpn J Infect Dis	58	1,2	2005
T. Matsuki, K. Isoda, R. Horai, A. Nakajima, Y. Aizawa, K. Suzuki, F. Ohsuzu, and Y. Iwakura.	Involvement of TNF-□ in the development of T cell-dependent aortitis in IL-1 receptor antagonist-deficient mice.	Circulation	112	1323-1331	2005
T. Ito-Ihara, T. Ono, F. Nogaki, K. Suyama, M. Tanaka, S. Yonemoto, A. Fukatsu, T. Kita, K. Suzuki, and E. Muso.	Clinical Efficacy of Intravenous Immunoglobulin for Patients with MPO-ANCA-associated Rapidly Progressive Glomerulonephritis.	Nephron Clin Pract.	102	35-42	2005
R. Suzuki, K. Tomizawa, K. Suzuki, M. Tanokura.	MPO-ANCA binding site on MPO molecule estimated from epitope mapping study and molecular modeling.	Bioimages	12	85-90	2005

M. Fujieda, K. Suzuki, H. Sato, M. Hattori, N. Wada, M. Tsuchiya, N. Okamoto, T. Murata, M. Matsudaira, M. Shimizu, K. Ohta, K. Naruse, S. Sugihara and H. Wakiguchi.	Epitope analysis of myeloperoxidase-specific antineutrophil cytoplasmic atoantibodies (MPO-ANCA) in childhood onset Graves'disease treated with propylthiouracil.	Clinical Nephrology	63	437-445	2005
T. Oharaseki, Y. Kameoka, F. Kura, A.S. Persad, K. Suzuki, S. Naoe.	Susceptibility loci to coronary arteritis in animal model of Kawasaki disease induced with Candida albicans-derived substances.	Microbiol.Immunol.	49	181-189	2005
N. Nagai-Miura, Y. Shingo, Y. Adachi, A. Ishida-Okawara, T. Oharaseki, K. Takahashi, S. Naoe, K. Suzuki and N. Ohno.	Induction of Coronary Arteritis with Administration of CAWS (Candida albicans Water-Soluble Fraction) Depending on Mouse Strains.	Immunopharmacol. Immunotoxicol.	26	527-543	2005
Watanabe-Akanuma, M. and T. Ohta	Inhibitory effects of NADH/NADPH in S9mix on photo-mutagenicity of thiabenda-zole following UVA-irradiation in E. coli.	Environ. Mutagen Res.	27	7-12	2005
Watanabe-Akanuma, M., T. Ohta, and Y. F. Sasaki	A novel genotoxic aspect of thia-bendazole as a photomutagen in bacteria and cultured human cells.	Toxicol. Lett.	158	213-219	2005
祖父尼俊雄，能美健彦，太田敏博，林真	遺伝毒性：DNA直接作用物質に閾値は存在するのか	環境変異原研究	27	61-73	2005
Ohta, T., S. Tokishita, M. Sakahira, K. Mochizuki, J. Kawase, and H. Yamagata	UV sensitivity and mutagenesis of the extremely thermophilic eubacterium Thermus thermophilus HB27.	Genes Environ.	In press		
Yamamoto A, Harada-Shiba M, Endo M, Kusakabe N, Tanioka H, Kato H, Shoji T.	The effect of ezetimibe on serum lipids and lipoproteins in patients with homozygous familial hypercholesterolemia undergoing LDL-apheresis therapy.	Atherosclerosis.	In press		

Umeda M, Harada-Shiba M, Uchida K, Nakayama Y.	Photo-Control of the polyplexen formation between DNA and photo-cation eneratable water-soluble polymers.	Current Drug Delivery.	2	207-214	2005
Nakayama Y, Masuda T, Nagaishi M, Hayashi M, Ohira M, Harada-Shiba M	High performance gene delivery polymeric vector: Nano-Structured cationic star polymers(star vectors).	Current Drug Delivery.	2	53-57	2005
N. Nishiyama, Arnida, W. -D. Jang, K. Date, K. Miyata, K. Kataoka	Photochemical enhancement of transgene expression by polymeric micelles incorporating plasmid DNA and dendrimer-based photosensitizer.	J. Drug Target.	In press		
N. Kanayama, S. Fukushima, N. Nishiyama, K. Itaka, W. -D. Jang, K. Miyata, Y. Yamasaki, U. Chung, K. Kataoka	PEG-based biocompatible block catiomer with high-buffering capacity for the construction of polyplex micelles showing efficient gene transfer toward primary cells.	ChemMedChem	In press		
R. Ideta, F. Tasaka, W. -D. Jang, N. Nishiyama, G. -D. Zhang, A. Harada, Y. Yanagi, Y. Tamaki, T. Aida, K. Kataoka	Nanotechnology-based photodynamic therapy for neovascular disease using a supramolecular nanocarrier loaded with a dendritic photosensitizer.	Nano Lett.	5 (12)	2426-2431	2005
K. Miyata, Y. Kakizawa, N. Nishiyama, Y. Yamasaki, T. Watanabe, M. Kohara, K. Kataoka	Freeze-dried formulations for in vivo gene delivery of PEGylated polyplex micelles with disulfide crosslinked cores to the liver.	J. Control. Release	109	15-23	2005
N. Nishiyama, A. Iriyama, W. -D. Jang, K. Miyata, K. Itaka, Y. Inoue, H. Takahashi, Y. Yanagi, Y. Tamaki, H. Koyama, K. Kataoka	Light-induced gene transfer from packaged DNA enveloped in a dendrimeric photosensitizer.	Nat. Mater.	4	934-941	2005

X. Yuan, Y. Yamasaki, A. Harada, K. Kataoka	Characterization of stable lysozyme-entrapped polyion complex (PIC) micelles with crosslinked core by glutaraldehyde.	Polymer	46	7749-7758	2005
Y. Bae, W. -D. Jang, N. Nishiyama, S. Fukushima, K. Kataoka	Multifunctional polymeric micelles with folate-mediated cancer cell targeting and pH-triggered drug releasing properties for active intracellular drug delivery.	Molecular BioSystems	1	242-250	2005
K. Osada, Y. Yamasaki, S. Katayose, K. Kataoka	A synthetic block copolymer regulates S1 nuclease fragmentation of supercoiled plasmid DNA.	Angew. Chem. Int. Ed. Engl	44	3544-3548	2005
S. Fukushima, K. Miyata, N. Nishiyama, N. Kanayama, Y. Yamasaki, K. Kataoka	PEGylated polyplex micelles from triblock catiomers with spatially ordered layering of condensed pDNA and buffering units for enhanced intracellular gene delivery.	J. Am. Chem. Soc.	127	2810-2811	2005
X. Yuan, A. Harada, Y. Yamasaki, K. Kataoka	Stabilization of lysozyme-incorporated polyion complex micelles by the ω-end derivatization of poly(ethylene glycol)-poly(α,β-aspartic acid) block copolymers with hydrophobic groups.	Langmuir	21	2668-2674	2005
S. Takae, Y. Akiyama, H. Otsuka, T. Nakamura, Y. Nagasaki, K. Kataoka	Ligand density effect on biorecognition by PEGylated gold nanoparticles: regulated interaction of RCA120 lectin with lactose installed to the distal end of tethered PEG strands on gold surface.	Biomacromolecules	6	818-824	2005
Y. Bae, N. Nishiyama, S. Fukushima, H. Koyama, Y. Matsumura, K. Kataoka	Preparation and biological characterization of polymeric micelle drug carriers with intracellular pH-triggered drug release property: Tumor permeability, controlled subcellular drug distribution, and enhanced in vivo antitumor efficacy.	Bioconjug. Chem.	16	122-130	2005

W. -D. Jang, N. Nishiyama, G. -D. Zhang, A. Harada, D. -L. Jiang, S. Kawauchi, Y. Morimoto, M. Kikuchi, H. Koyama, T. Aida, K. Kataoka	Supramolecular nanocarrier of anionic dendrimer porphyrins with cationic block copolymers modified with poly(ethylene glycol) to enhance intracellular photodynamic efficacy.	Angew. Chem. Int. Ed. Engl.	44	419-423	2005
H. Cabral, N. Nishiyama, S. Okazaki, H. Koyama, K. Kataoka	Preparation and biological properties of dichloro(1,2-diaminocyclohexane)platinum(II) (DACHPt)-loaded polymeric micelles.	J. Control. Release	101	223-232	2005
Kurokawa Y, Honma K, Takemasa I, Nakamori S, Kita-Matsuo H, Motoori M, Nagano H, Dono K, Ochiya T, Monden M, Kato K	Central genetic alterations common to all HCV-positive, HBV-positive and non-B, non-C hepatocellular carcinoma: A new approach to identify novel tumor markers.	Int J Oncol	In press		
Fukasawa M, Morita S, Kimura M, Horii T, Ochiya T, Hatada I	Genomic imprinting in Dicer1-hypomorphic mice.	Cytogenet Genome Res.	In press		
Banas A, Quinn G, Yamamoto Y, Teratani T, Ochiya T	"Stem cells into liver"-Basic research and potential clinical application.	Adv. Exp. Med. Mol. Biol	In press		
Takeshita F, Minakuchi Y, Nagahara S, Honma K, Sasaki H, Hirai K, Teratani T, Namatame N, Yamamoto Y, Hanai K, Kato T, Sano A, Ochiya T.	Efficient delivery of small interfering RNA to bone-metastatic tumors by using atelocollagen in vivo.	Proc Natl Acad Sci USA.	102	12177-12182	2005
Yanagihara K, Takigahira M, Tanaka H, Komatsu T, Fukumoto H, Koizumi F, Nishio K. Ochiya T, Ino Y, Hirohashi S.	Development and biological analysis of peritoneal metastasis mouse models for human scirrhous stomach cancer.	Cancer Sci.	96	323-332	2005

Saito S, Honma K, Kita-Matsuo H, Ochiya T, Kato K.	Gene expression profiling of cerebellar development with high-throughput functional analysis	Physiol Genomics.	22	8-13	2005
Teratani T, Quinn G, Yamamoto Y, Sato T, Yamanokuchi H, Asari A, Ochiya T.	Long-term maintenance of liver-specific functions in cultured ES cell -derived hepatocytes with hyaluronan sponge.	Cell Transplant	14	629-635	2005
Yamamoto Y, Teratani T, Yamamoto H, Quinn G, Murata S, Ikeda R, Kinoshita K, Matsubara K, Kato T, Ochiya T.	Recapitulation of in vivo gene expression during hepatic differentiation from embryonic stem cells	Hepatology	42	558-567	2005
Teratani T, Yamamoto H, Aoyagi K, Sasaki H, Asari A, Quinn G, Sasaki H, Terada M, Ochiya T.	Direct hepatic fate specification from mouse embryonic stem cells.	Hepatology	41	836-846	2005
落谷孝広	siRNA デリバリーシステムのがん治療への応用	Pharm Tech JAPAN	21	104-107	2005
竹下文隆、落谷孝広	アテロコラーゲンによる遺伝子治療用ベクターの生体内制御	Molecular Medicine	42	292-297	2005
竹下文隆，落谷孝広	アテロコラーゲンによるがん治療を目的とした siRNA の in vivo デリバリーシステム.	RNA 工学の最前線		88-96	2005

Microbiol. Immunol., **49**(5), 461–470, 2005

Editor-Communicated Paper

Simultaneous Multicolor Detection System of the Single-Molecular Microbial Antigen with Total Internal Reflection Fluorescence Microscopy

Akiyoshi Hoshino[1,2], Kouki Fujioka[1], Noriyoshi Manabe[1], Shun-ichi Yamaya[1], Yoji Goto[3], Masato Yasuhara[2], and Kenji Yamamoto*[,1,2]

[1]*Department of Medical Ecology and Informatics, Research Institute, International Medical Center of Japan, Shinjuku-ku, Tokyo 162–8655, Japan,* [2]*Department of Pharmacokinetics and Pharmacodynamics, Hospital Pharmacy, Tokyo Medical and Dental University Graduate School, Bunkyo-ku, Tokyo 113–8519, Japan, and* [3]*Research Center for Biologicals, The Kitasato Institute, Kitamoto, Saitama 364–0026, Japan*

Communicated by Dr. Hidechika Okada: Received February 25, 2005. Accepted March 1, 2005

Abstract: **Immunological diagnostic methods have been widely performed and showed high performance in molecular and cellular biology, molecular imaging, and medical diagnostics. We have developed novel methods for the fluorescent labeling of several antibodies coupled with fluorescent nanocrystal QDs. In this study we demonstrated that two bacterial toxins, diphtheria toxin and tetanus toxin, were detected simultaneously in the same view field of a cover slip by using directly QD-conjugated antibodies. We have succeeded in detecting bacterial toxins by counting luminescent spots on the evanescent field with using primary antibody conjugated to QDs. In addition, each bacterial toxin in the mixture can be separately detected by single excitation laser with emission band pass filters, and simultaneously *in situ* pathogen quantification was performed by calculating the luminescent density on the surface of the cover slip. Our results demonstrate that total internal reflection fluorescence microscopy (TIRFM) enables us to distinguish each antigen from mixed samples and can simultaneously quantitate multiple antigens by QD-conjugated antibodies. Bioconjugated QDs could have great potentialities for in practical biomedical applications to develop various high-sensitivity detection systems.**

Key words: **Simultaneous multicolor detection, Single-molecular microbial antigen, TIRFM, Quantum dot**

The high sensitivity detection system, which detects the smaller amounts of chemicals and biomolecules, is a prospective technology and can be applied not only for medical application but for the preparations and responses in case of emergency in various fields; environmental technology, water poisoning, safety of food and drug supply, and public health security such as preparation against bioterrorism. However, a lot of processes are required to detect these smaller amounts of harmful substances. Hence, there is a problem to require much time in detection of biomolecules.

The immunological diagnostic methods were widely performed in the medical field. In these cases, almost all of the samples are provided as blood, tissue, exudation fluid, or excrement, and the antigen-antibody reaction was commonly performed as the detection method in addition to the colorimetric methods. In this article we developed a high sensitive and quick antigen detecting system using the fluorescence nanocrystal quantum dots (QDs) about a substance detrimental to the biomolecules, such as a bacterial toxin that caused food poisoning or bioterrorism. In order to detect bacterial toxins sensitively and quickly, we adapted the fluorescence-ELISA using QDs to the origin of evanescent microscopy. In this system, the fluorescence of the QD-conjugated antibody, which detects bacterial toxins, is placed on the evanescent filed, resulted in detecting bacterial toxins countable by single molecules. Imaging

Address correspondence to Dr. Kenji Yamamoto, Department of Medical Ecology and Informatics, Research Institute, International Medical Center of Japan, Toyama 1–21–1, Shinjuku-ku, Tokyo 162–8655, Japan. Fax: +81–3–3202–7364. E-mail: backen@ri.imcj.go.jp

Abbreviations: QD, quantum dot; TIRFM, total internal reflection fluorescent microscopy.

of single fluorescent molecules has been achieved using an objective-type total internal reflection fluorescence microscopy (TIRFM). TIRFM selectively illuminates the aqueous phase immediately adjacent to a glass interface with an exponentially decaying excitation called evanescent stages (1, 23, 24). In TIRFM, also called evanescent wave microscopy, the excitation light typically penetrates <150 nm above the reflecting surface and is ideal for studying the surface of the cellular processes such as cell adhesion.

Nanocrystal quantum dots (QDs) are ultrafine fluorescent-emitting particles that consist of CdSe/ZnS-core/shell semiconductor nanoparticles. QDs have the potential to be applied to bioimaging due to their higher and far longer fluorescence. QDs were widely used in biotechnology and medical applications (3, 4, 7–9, 17–22, 27, 28). Several applications have demonstrated that QDs were adapted for immunoassay and diagnostics (2, 9, 10, 16, 25). QDs have several advantages over organic fluorophores. QDs show high luminance, resistance to photobleaching, a range of exciting wavelength from ultra violet to red that depends on the size of the particles, and cover a range of fluorescent wavelengths from blue to red that can be excited using a mercury arc lamp. At present, many organic fluorophores were used for TIRFM imaging, but experiments using organic dyes are unsuitable for extended periods of bioimaging observations because organic fluorophores tend to quench rapidly (5). In contrast, QDs are stabilized over a far longer exposure-time to light and can emit a fluorescence of high luminosity under almost the equivalent condition as the conventional organic fluorescence probes (15). In this study, we performed the detection of diphtheria toxin and tetanus toxoid by different color-emitting QD-conjugated antibodies, and visualized each toxin within the same view field.

Materials and Methods

Antigens, antibodies, and reagents. Four target proteins; casein from bovine milk, equine cytochrome-*c*, lysozyme, and ovalbumin from chicken egg, were purchased from Sigma-Aldrich (St. Louis, Mo., U.S.A.). Antibodies for lysozyme and ovalbumin were purchased from Rockland, Inc. (Gilbertsville, Penn., U.S.A.), ones for cytochrome-*c* was from Nordic Immunological Laboratories (Tilburg, Netherlands). Diphtheria toxin and anti-diphtheria toxin antibody (human) were provided by Toyo Public Health College (Tokyo). Anti-tetanus toxin antibody was purchased from Biogenesis (Poole, England, U.K.). Tetanus toxin, human HBs antigen, and sheep antiserum for HBs antigen were provided by Kitasato Institute (Tokyo). Anti-HBs antibody was purified by Hi-Trap protein G column (Amersham Pharmacia, Uppsala, Sweden). All the antibodies used in this study were directly labeled with QDs as described below.

Preparation of antibody-conjugated QDs. ZnS-capped CdSe core-shell nanocrystal QDs (fluorescence wavelength: approximately 642 nm emitted red, and approximately 518 nm emitted green), were enfolded into the micelle of *n*-trioctylphosphine oxide (TOPO), according to general methods (6, 12). Then the hydrophilic QDs (carboxyl-QDs) were produced by thiol exchange reaction (13). The antibodies described above were conjugated to QDs by the two-step reaction as described previously (14). QD solution was primarily mixed with cysteine solution in coexistent with 1-ethyl-3-(3-dimethylaminopropyl)-carbodiimide cross-linking reagents (EDC, Pierce Biotechnology, Rockfold, Ill., U.S.A.) and mixed under the chilled condition, and secondarily coupled with target antibodies by attaching succinimidyl 4-(*N*-maleimidomethyl)cyclohexane-1-carboxylate (SMCC, Pierce Biotech) under sonicated condition. The products were purified using Superdex200® gel filtration column (Amersham Biosciences, Piscataway, Ill., U.S.A.). Finally, purified QD-peptide conjugates were concentrated by Ultrafree®-biomax centrifugal filter devices (Millipore, Bedford, Mass., U.S.A.). To analyze the protein content of QD-conjugated peptides, conjugated QDs were plated to 96-well microplate and RC-DC Protein Assay reagent (Bio-Rad, Hercules, Calif., U.S.A.) was added. After incubation for 1 hr, 650 nm absorbance was measured by microplate reader (Bio-Rad). Hydrophilic QD was used as negative control.

Fluorescent immunoassays. 0.12 mm-thickness coverslips (Matsunami Glass Industries, Japan) were precoated with poly-L-lysine (Peptide Institute Co., Ltd., Osaka, Japan), to avoid the non-specific binding of QDs on the glass. Then target peptides were dissolved in bicarbonate buffer (pH 8.2) and plated on the coverslip at an adequate concentration. After incubation, blocking reaction was performed with 0.2% gelatin in carbonate buffer at 37 C for 30 min. Next, QD-labeled antibodies were added to the plate and incubated at 37 C for 30 min. After washed with PBS 5 times, fluorescence was detected by TIRFM. Quantitation of antigen absorbed on the coverslip was detected by performing ELISA on the glass. Briefly, the coverslip with target peptide was treated with unlabeled primary antibody for 30 min (the same antibody used for QD-conjugation) and secondary reacted with HRP-conjugated secondary antibody for 30 min again (Goat anti-human or rabbit IgGs from Zymed Laboratories, South San Francisco,

Calif., U.S.A.). Then, TMB substrate (KPL Corp., Gaithersburg, Md., U.S.A.) was added to the coverslip. After stopping reaction, 100 μl of colored solution was transferred to the 96-well multiplate. Four-hundred and fifty nanometer absorbance (reference; 650 nm) was measured by microplate reader (Bio-Rad). Fluorescence emission on the multiwell plate was measured by fluorescent microplate reader (Fluoroskan Ascent, Thermo Electron Corp., Wattham, Mass., U.S.A.). ELISA on the MaxiSorp® 96-well microplate (Nalge Nunc, Naperville, Ill., U.S.A.) was used as standard curve.

Multi-channel total internal reflection fluorescence microscopy imaging. Objective-based multi-channel TIRFM was obtained by directing an argon ion 488 nm laser through dichroic mirrors (DM505) and emission filters on an Olympus IX-70 microscope. The laser beam was on the coverslip at 58.4–64.2 degree to the optical axis giving a decay constant of the evanescent field of 48–62 nm. The beam was focused on the periphery of the back focal plane of a 100× objective with *NA* of 1.65 with high refractive index immersion oil (Olympus Corp., Tokyo). The filter cube contained a 488/10 laser clean-up filter in the excitation position, and emission signals were separated using two kinds of optical splitters; Ch1 was with 510–550 bandpass, and Ch2 was with >610 longpass emission filters; the red (Ch2) and green (Ch1) images were simultaneously imaged side by side on a CCD camera. Images were acquired, and the raw stacks were split into single channels using MetaMorph® software (Universal Imaging Corp., Marlow, Buckinghamshire, U.K.).

Results and Discussion

Fluorescent QDs are suitable for multiplexed analyzing tool by using those properties that emits luminescence that depends on their particle size. Multiplexed fluoroimmunoassays using QD has already reported (10, 11). In this study we try to detect antigen-antibody reaction at single molecular level and to achieve the high-sensitive *in situ* antigen quantitation using by an evanescent microscopy. To confirm the assay performance, we first examined the simulation for the detection of each antigen by using ovalbumin, lysozyme, cytochrome-*c*, and antibodies for those antigens. First, ovalbumin was dissolved in bicarbonate buffer contained 1 μg/ml casein, and 100 μl of solution plated on the cover slip at 1, 0.1, and 0.01 μg/ml. Absorbed ovalbumin molecules on the evanescent field were detected by QD-conjugated anti-ovalbumin antibody (Fig. 1a). In TIRFM imaging, every antigen was visible as a fluorescent spot. The fluorescent intensity on TIRFM was measured by counting luminescent spots of the 5 μm×5 μm view field on TIRFM images (Fig. 1b). By using QD-labeled secondary antibody, non-linear fluorescence was observed by microplate reader. On the other hand, linear response still remained on the signal of TIRFM images. Thus, antigen detection using TIRFM has advantages with the exclusion of non-specific signal out of evanescent view fields.

Next, we assessed detection of specific antigen from the mixture of several antigens. The mixture solution of casein, cytochrome-*c*, and ovalbumin was plated on the coverslip. Next ovalbumin was detected by QD-conjugated anti-ovalbumin antibodies (Fig. 2a, left). Fluorescent spots emitted from albumin-antibodies were observed at dose dependent manner. In contrast, luminescent spots from cytochrome-antibodies were not affected by the dose of ovalbumin but by cychrome (Fig. 2a, right). The same pattern was also detected by cytochrome (Fig. 2b) and casein (data not shown). Then we compare the antigen detection by colorimetric method with HRP-conjugated antibody and by QD-conjugated antibody on TIRFM. A conventional ELISA was performed on the glass-based plate under the same condition performed in Fig. 2, and 450 nm absorbance of colored TMB peroxidase reagents was measured by microplate reader (Fig. 3, filled symbols). These results indicated that the specific antigen could be also detected separately on the evanescent view fields at high performance as well as ELISA.

Then we tried simultaneous detection of two antigens on the same plate by green- and red-emitted QD conjugated antibodies. The mixture of ovalbumin and cytochrome-*c* was plated on the cover slip at the indicated concentration. Ovalbumin and cytochrome-*c* were simulataneously detected by QD640 (emitted red)-labeled anti-ovalbumin or QD520 (emitted green) labeled anti-cytochrome-*c* antibodies. Without using any filters, luminescences from QD520 and QD640 were not distinguished from each other and observed as yellow (merged) images in the view field. In contrast, TIRFM images can detect both signals from QD520 and QD640 simultaneously as luminescent spots (Fig. 4). In addition, emission signals of the green and the red were simultaneously detected by two kinds of optical splitters. Then ovalbumin and cytochrome-*c* were simultaneously detected by the mixture of anti-ovalbumin (QD640) and anti-cytochrome-*c* (QD520) antibodies at dose-dependent manner. Luminescence was divided to red and green channels as described in Fig. 4. These results suggested that these two antigens can be simultaneously detected as green and red luminescent spots and be quantitated by counting luminescence spots by using TIRFM imaging.

Next, we examined whether microbial antigen also

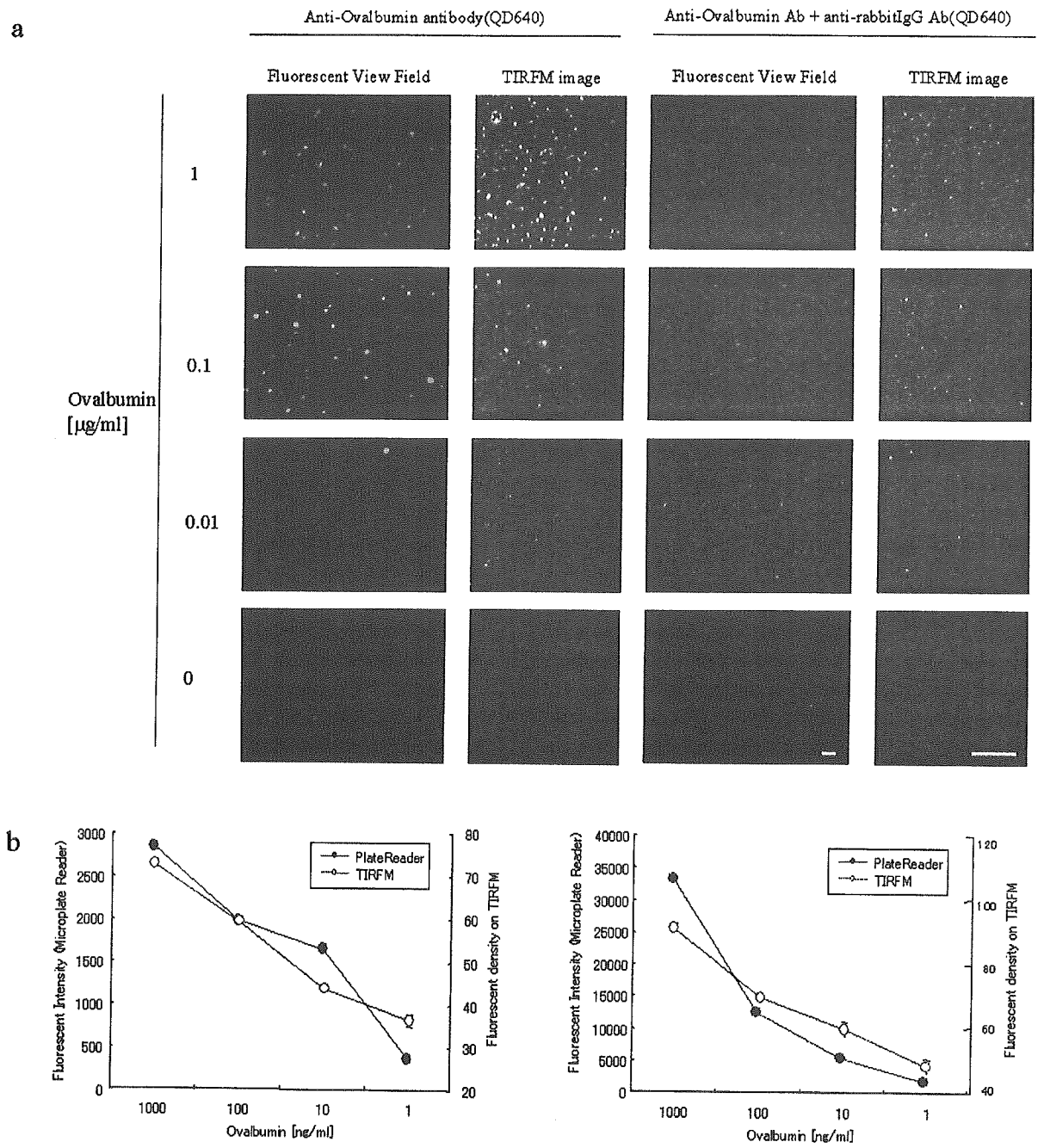

Fig. 1. Antigen detection by QD-conjugated antibody on the evanescent field. (a) TIRFM and fluorescent imaging of antigen. Ovalbumin solution was plated on the cover slip at indicated concentration. Absorbed ovalbumin molecules on the evanescent field were detected by QD-conjugated anti-ovalbumin antibody. The images represent one out of three performed. Bars indicate 10 μm. (b) The fluorescence intensity measured by fluorescent microplate reader is given on the left scale of *y*-axis and the fluorescent counts on TIRFM are on the right scale of *y*-axis, respectively. Fluorescence density was performed by counting luminescent spots of the 5 μm×5 μm view field on TIRFM images. The data are presented as the mean±standard deviation (n=3). Open circles indicate TIRFM counts, and closed circles are fluorescent intensity, respectively.

can be detected by TIRFM. At first, human hepatitis virus antigen (HBs) was plated on the cover slip and detected by QD-conjugated anti-HBs antibody (Fig. 6a). Viral antigen was also detected by TIRFM imaging. Detection sensitivity of HBs by ELISA was shown in Fig. 6b. The sensitivity of ELISA method shows 10 times higher than that of TIRFM imaging. This is caused by the non-specific luminescent spots at background level.

Then we assessed the simultaneous detection of two bacterial toxins by TIRFM. We tried to image the antigen-antibody reaction of diphtheria toxin and tetanus

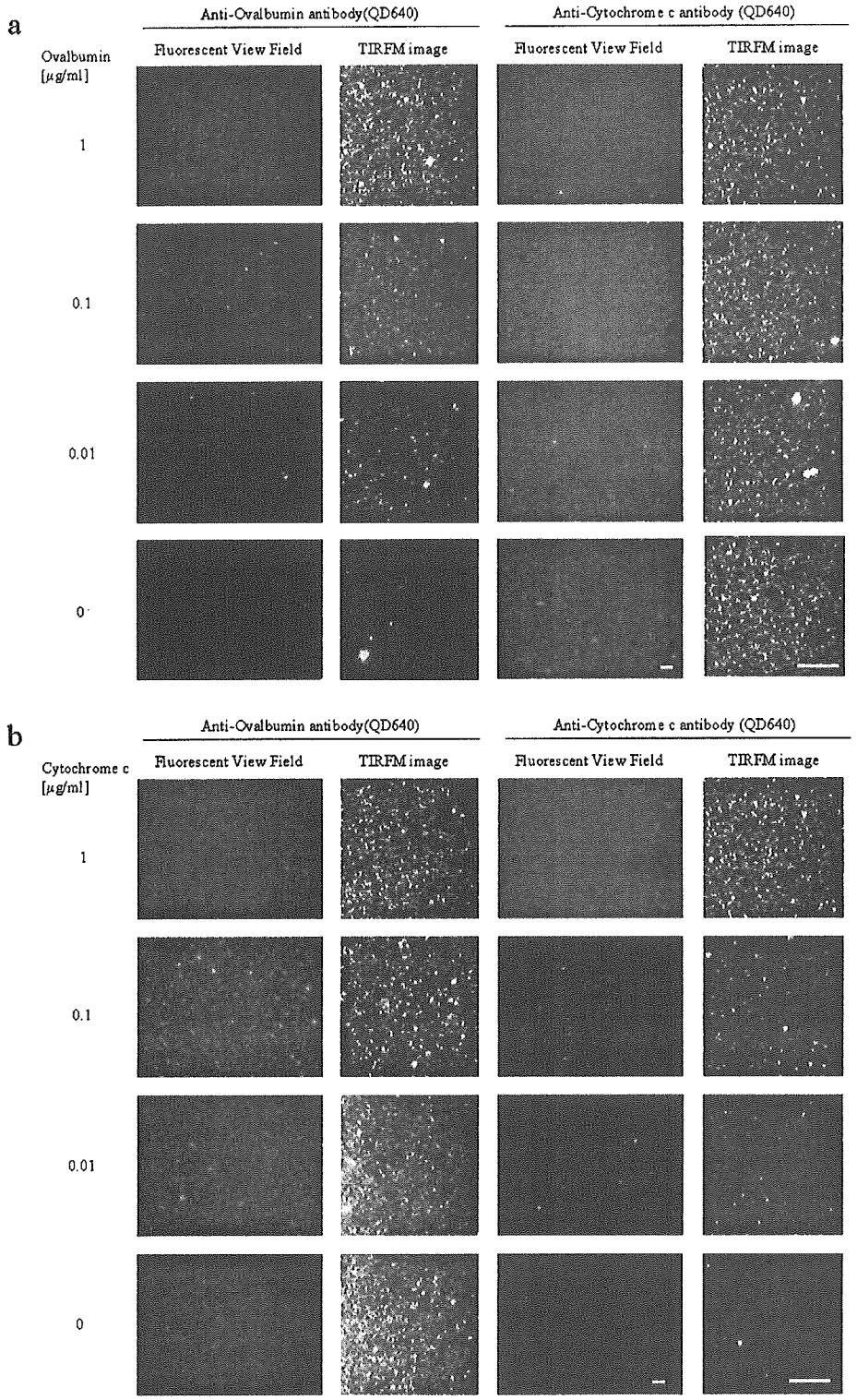

Fig. 2. Two antigens on the evanescent field were detected by QD-conjugated antibody. The mixture of ovalbumin and cytochrome-*c* was plated on the cover slip at indicated concentration. Each antigen was separately detected by QD-conjugated anti-ovalbumin (a) or anti-cytochrome-*c* (b) antibodies, as shown in Fig. 1. Shown are data of a representative experiment (n=3). Bars indicate 10 μm.

toxin. Mixture of two bacterial toxins were plated on the cover slip at indicated concentrations, and detected by anti-diphtheria toxin (QD520) and anti-tetanus toxin (QD640) antibodies (Fig. 7a). At the same time, detection sensitivity of diphtheria and tetanus toxins by ELISA was also performed on the glass-base dishes

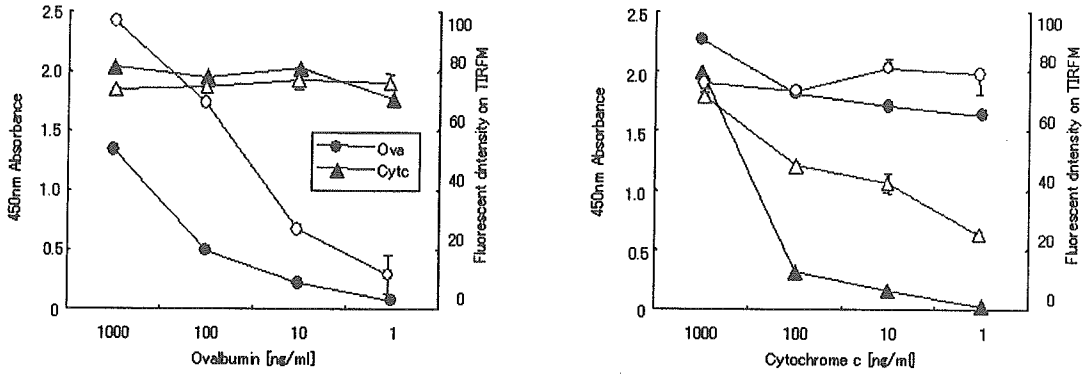

Fig. 3. Comparison of antigen detection by colorimetric method with HRP-conjugated antibody and by QD-conjugated antibody on TIRFM. ELISA of two antigens on the glass-based plate was performed. Absorbance of peroxidase reagents is given on the left scale of y-axis. Values are the means±standard deviation of duplicate experiments. Results were reproduced in three separate experiments. As described in Fig. 1b, the fluorescent counts on TIRFM are on the right scale, respectively. Filled symbols indicated the results of ELISA. Circles and triangles mean ovalbumin and cytochrome-*c*, respectively.

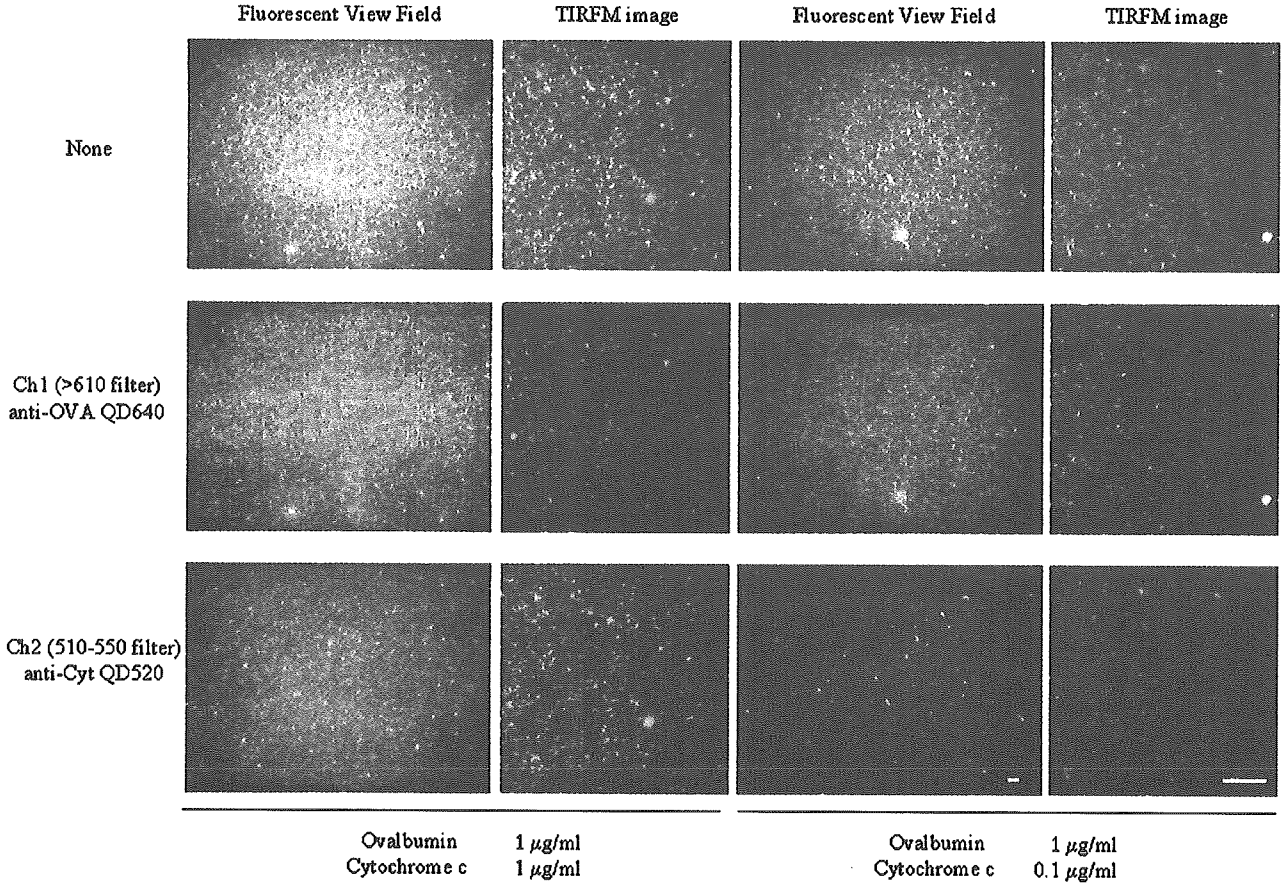

Fig. 4. Two antigens on the same plate were simultaneously detected by green- and red-emitted QD conjugated antibodies. The mixture of ovalbumin and cytochrome-*c* was plated on the cover slip at indicated concentration. Ovalbumin and cytochrome-*c* were simultaneously detected by QD640 (emitted red)-labeled anti-ovalbumin or QD520 (emitted green) labeled anti-cytochrome-*c* antibodies. Luminescence was divided to indicated channels according to the emission wavelengths of QDs. Bars indicate 10 μm. None: images without using emission filters.

(Fig. 7b). Anti-diphtheria toxin (human) or anti-tetanus toxin (rabbit) was added, and toxins were detected by human or rabbit HRP-conjugated secondary antibodies. These results suggested that TIRFM method does not excel the conventional detection system in the sensitivity or certainty. But two bacterial antigens can also be simultaneously detected and quantitated by counting luminescence spots, implying that TIRFM system was

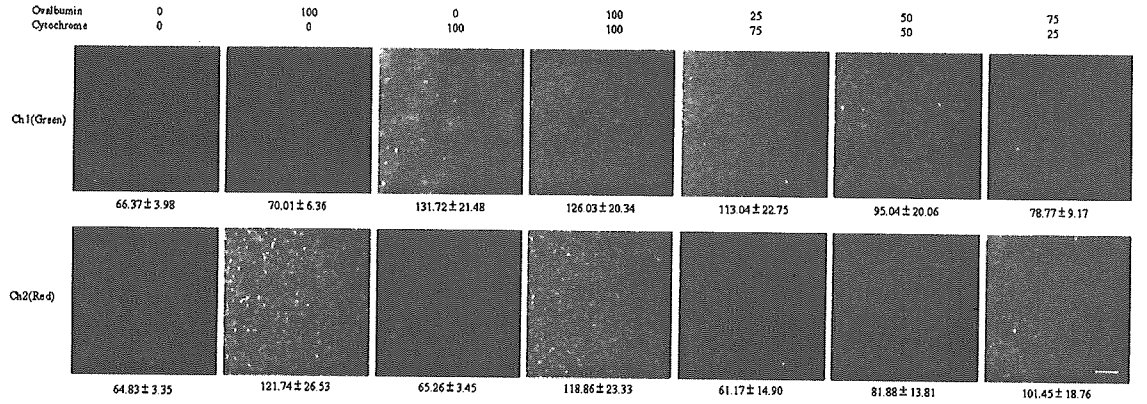

Fig. 5. Two antigens on the same plate were simultaneously detected by green- and red-emitted QD conjugated antibodies. Ovalbumin and cytochrome-*c* were simultaneously detected by the mixture of anti-ovalbumin (QD640) and anti-cytochrome-*c* (QD520) antibodies. Luminescence was divided to red and green channels as described in Fig. 4. Bars indicate 10 μm.

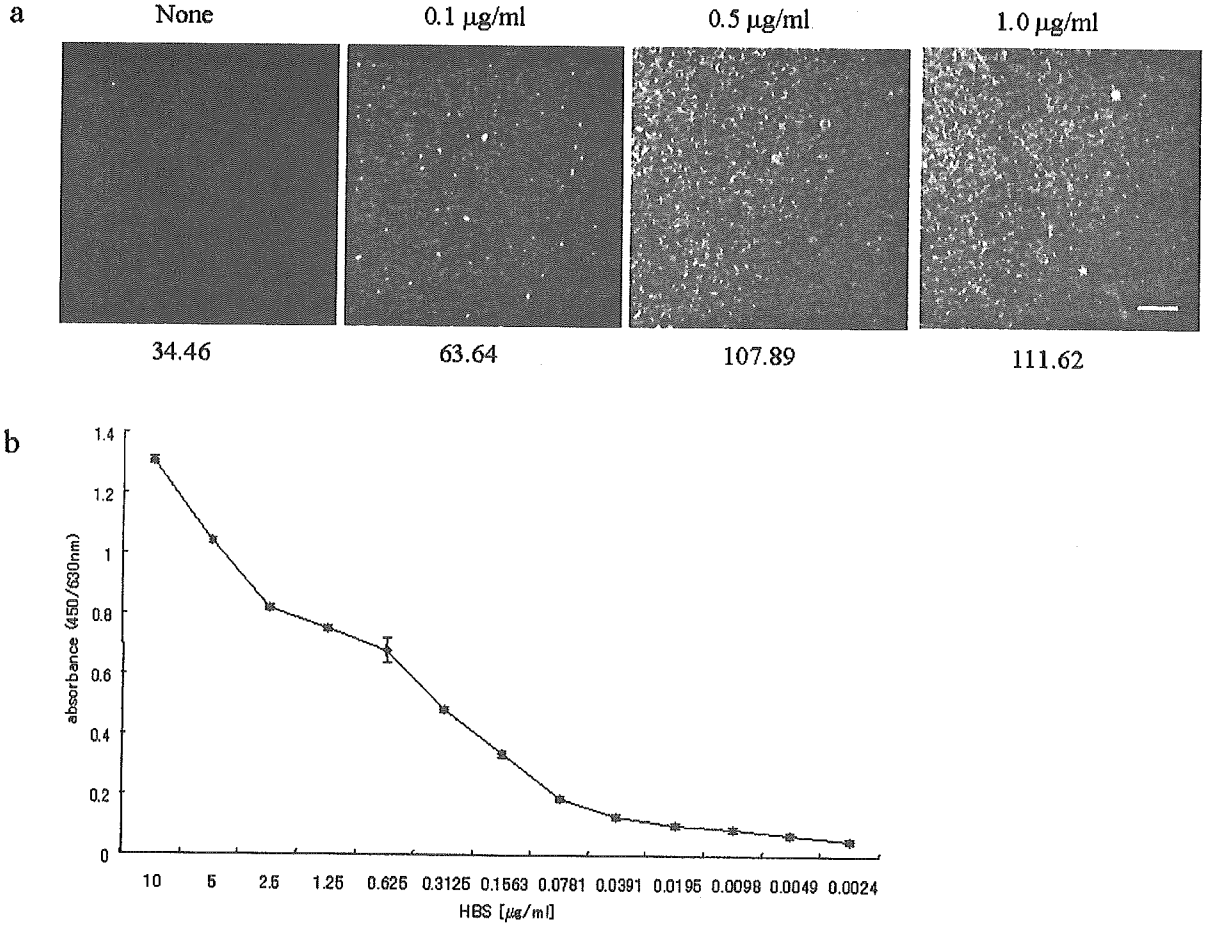

Fig. 6. Detection of viral antigen by TIRFM. (a) TIRFM imaging of human hepatitis virus antigen (HBs). HBs antigen was plated on the cover slip and detected by QD-conjugated anti-HBs antibody. Bars indicate 10 μm. Detection sensitivity of HBs by ELISA was shown in (b). The data are presented as the mean±standard deviation of duplicated samples.

suitable for a multicolor and high-speed detection system.

It is extremely important to determine pathogenic bacteria rapidly and sensitively in biotechnology, medical diagnosis, and the current fight against bioterrorism. Current analysis techniques either lack ultrasensitivity or take a long time for analysis. In this method, the bioconjugated QDs provides an extremely high fluorescent signal for bioanalysis and can be easily incorporated with recognition of molecules. This system,

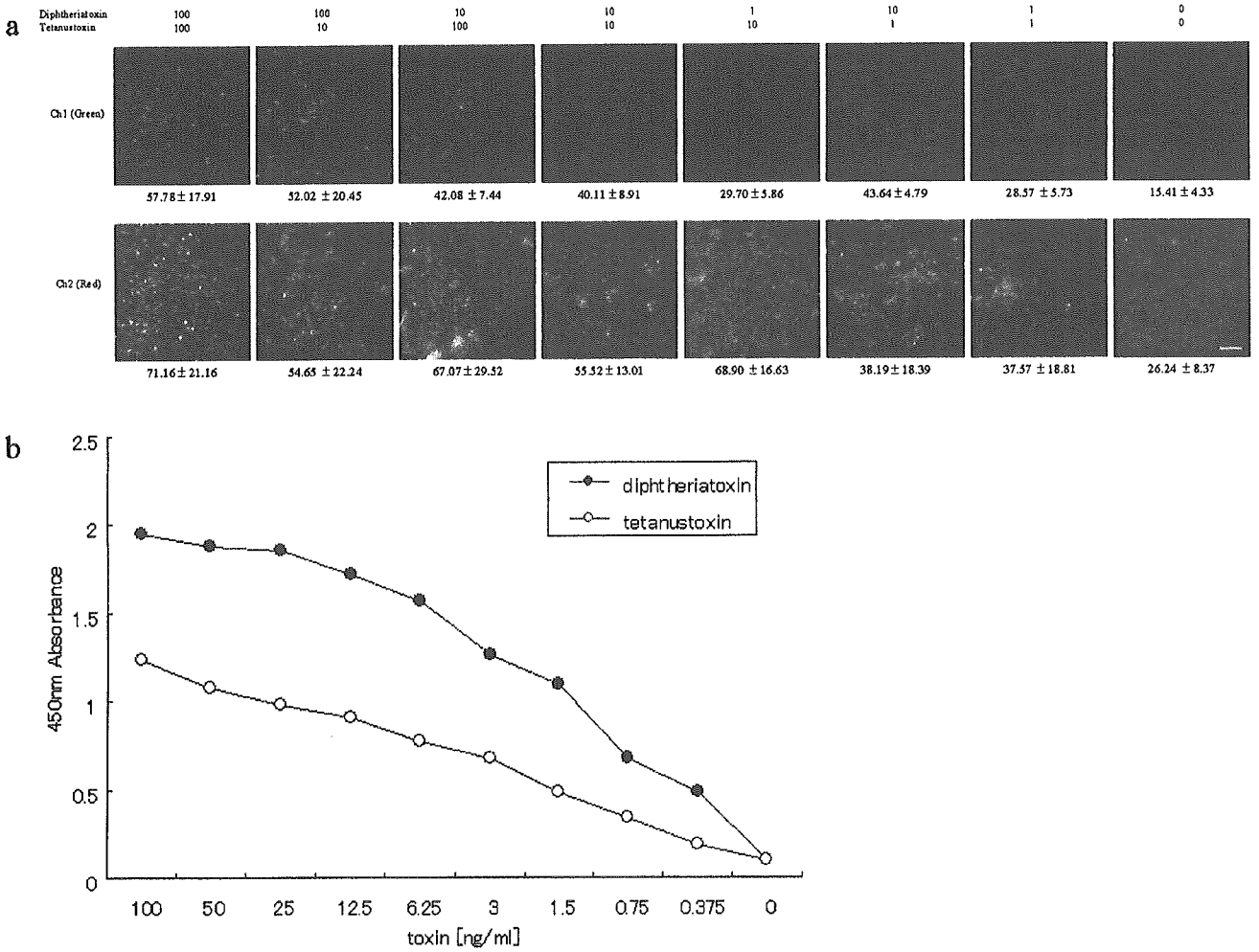

Fig. 7. Simultaneous detection of two bacterial toxins by TIRFM. (a) TIRFM imaging of diphtheria toxin and tetanus toxin. Mixture of two bacterial toxins were plated on the cover slip at indicated concentrations, and detected by anti-diphtheria toxin (QD520) and anti-tetanus toxin (QD640) antibodies. Bars indicate 10 μm. (b) ELISA detection sensitivity of diphtheria and tetanus toxins. Anti-diphtheria toxin (human) or anti-tetanus toxin (rabbit) was added to 96-well plate. Toxins were detected by human or rabbit HRP-conjugated secondary antibodies. The data are presented as the mean±standard deviation of duplicated samples.

which was improved based on the recognition function of an antibody, has the same advantages as conventional immunoassay, which can measure specific target molecules with sufficient specificity. But unfortunately this system reflects the weak point of immunoassays. The sandwiching method is used commonly and widely in immunoassays; another epitope of target protein is recognized apart from the fixed antibody after catching the target protein. In general technique, detection was dependent on the secondary antibody that combines biotin or that were the specific antibody to the immunoglobulin of an immunized animal (e.g.; anti-human IgG), and then finally detected by the colorimetric substrate, the chemiluminescent reagents, or the fluorescence such as Alexa®fluor or CyChrome® dyes (26). Enhancement of assay performance has been achieved by several methods. Huang reported that simultaneous detection of multiple proteins was demonstrated by an array-based enzyme-linked immunosorbent assay (ELISA) and enhanced chemiluminescence (ECL) (16), and Mattoussi et al., demonstrated by fluorescent probes by QDs (11). Almost all of the advanced assay use secondary antibody to enhance the sensitivity by using sandwiching method (29). However in a TIRFM detection system by the sandwiching method, quantum dot antibody is hard to be excited because secondary antibody exists far from the limit of distance on evanescent field.

This system is a novel immunological diagnostic methods, which can be expected to improve the high-throughput diagnosis that will be performed quickly and simply by this method compared with the conventional method. However, this method does not excel the conventional one in the sensitivity or certainty. As a

method of applying a system, the reaction system is integrated in the small cartridge and miniaturized to the portable size. For example, we expected that the system could make a significant contribution to judge the authenticity at high-speed and high sensitivity in the case of suspicions of the bioterrorism.

We are grateful to Dr. Shun-ichi Yamaya (Toyo Public Health College) for providing diphtheria toxin and anti-diphtheria toxin antibody (human). We thank Dr. Wayne Dawson (Chiba Institute of Technology, Chiba, Japan) for valuable help for proofreading, and Mr. Kazuyuki Ito and Mr. Kimiyoshi Arakawa (Department of Medical Ecology, Research Institute, IMCJ) for valuable help.

References

1) Akerman, M.E., Chan, W.C., Laakkonen, P., Bhatia, S.N., and Ruoslahti, E. 2002. Nanocrystal targeting *in vivo*. Proc. Natl. Acad. Sci. U.S.A. **99**: 12617–12621.
2) Axelrod, D. 1989. Total internal reflection fluorescence microscopy. Methods Cell Biol. **30**: 245–270.
3) Bruchez, M., Jr., Moronne, M., Gin, P., Weiss, S., and Alivisatos, A.P. 1998. Semiconductor nanocrystals as fluorescent biological labels. Science **281**: 2013–2016.
4) Chan, W.C., and Nie, S. 1998. Quantum dot bioconjugates for ultrasensitive nonisotopic detection. Science **281**: 2016–2018.
5) Chan, W.C., Maxwell, D.J., Gao, X., Bailey, R.E., Han, M., and Nie, S. 2002. Luminescent quantum dots for multiplexed biological detection and imaging. Curr. Opin. Biotech. **13**: 40–46.
6) Dabboussi, B.O., Rodriguez-Viejo, J., Mikulec, F.V., Hein, J.R., Mattoussi, H., Ober, R., Jensen, K.F., and Bawendi, M.G. 1997. (CdSe)ZnS core-shell quantum dots; synthesis and characterization of size series of highly luminescent nanocrystallites. J. Phys. Chem. **101**: 9463–9475.
7) Dubertret, B., Skourides, P., Norris, D.J., Noireaux, V., Brivanlou, A.H., and Libchaber, A. 2002. *In vivo* imaging of quantum dots encapsulated in phospholipid micelles. Science **298**: 1759–1762.
8) Gao, X., Chan, W.C., and Nie, S. 2002. Quantum-dot nanocrystals for ultrasensitive biological labeling and multicolor optical encoding. J. Biomed. Optics **7**: 532–537.
9) Gao, X., Cui, Y., Levenson, R.M., Chung, L.W.K., and Nie, S. 2004. *In vivo* cancer targeting and imaging with semiconductor quantum dots. Nat. Biotechnol. **22**: 969–976.
10) Goldman, E.R., Anderson, G.P., Tran, P.T., Mattoussi, H., Charles, P.T., and Mauro, J.M. 2002. Conjugation of luminescent quantum dots with antibodies using an engineered adaptor protein to provide new reagents for fluoroimmunoassays. Anal. Chem. **74**: 841–847.
11) Goldman, E.R., Clapp, A.R., Anderson, G.P., Uyeda, H.T., Mauro, J.M., Medintz, I.L., and Mattoussi, H. 2004. Multiplexed toxin analysis using four colors of quantum dot fluororeagents. Anal. Chem. **76**: 684–688.
12) Hines, M.A., and Guyot-Sionnest, P. 1996. Synthesis and characterization of strongly luminescing ZnS-capped CdSe nanocrystals. J. Phys. Chem. **100**: 468–471.
13) Hoshino, A., Fujioka, K., Oku, T., Suga, M., Sasaki, Y.F., Ohta, T., Yasuhara, M., Suzuki, K., and Yamamoto, K. 2004. Physicochemical properties and cellular toxicity of nanocrystal quantum dots depend on their surface modification. Nano Lett. **4**: 2163–2169.
14) Hoshino, A., Fujioka, K., Oku, T., Suga, M., Nakamura, S., Yamaguchi, Y., Suzuki, K., Yasuhara, M., and Yamamoto, K. 2004. Quantum dots targeted to the assigned organelle in living cells. Microbiol. Immunol. **48**: 669–675.
15) Hoshino, A., Hanaki, K., Suzuki, K., Yamamoto, K. 2004. The applications T-lymphoma labeled with fluorescent quantum dots to cell trafficking markers in a mouse body. Biochem. Biophys. Res. Commun. **314**: 46–53.
16) Huang, R.P. 2001. Simultaneous detection of multiple proteins with an array-based enzyme-linked immunosorbent assay (ELISA) and enhanced chemiluminescence (ECL). Clin. Chem. Lab. Med. **39**: 209–214.
17) Ishii, D., Kinbara, K., Ishida, Y., Ishii, N., Okochi, M., Yohda, M., and Aida, T. 2003. Chaperonin-mediated stabilization and ATP-triggered release of semiconductor nanoparticles. Nature **423**: 628–632.
18) Jaiswal, J.K., Mattoussi, H., Mauro, J.M., and Simon, S.M. 2003. Long-term multiple color imaging of live cells using quantum dot bioconjugates. Nat. Biotechnol. **21**: 47–51.
19) Larson, D.R., Zipfel, W.R., Williams, R.M., Clark, S.W., Bruchez, M.P., Wise, F.W., and Webb, W.W. 2003. Water-soluble quantum dots for multiphoton fluorescence imaging *in vivo*. Science **300**: 1434–1436.
20) Mattoussi, H., Mauro, J.M., Goldman, E.R., Anderson, G.P., Sundar, V.C., Mikulec, F.V., and Bawendi, M.G. 2000. Self-assembly of CdSe-ZnS quantum dot bioconjugates using an engineered recombinant protein. J. Am. Chem. Soc. **122**: 12142–12150.
21) Rosenthal, S.J., Tomlinson, I., Adkins, E.M., Schroeter, S., Adams, S., Swafford, L., McBride, J., Wang, Y., DeFelice, L.J., and Blakely, R.D. 2002. Targeting cell surface receptors with ligand-conjugated nanocrystals. J. Am. Chem. Soc. **124**: 4586–4594.
22) Shubeita, G.T., Sekatskii, S.K., Dietler, G., Potapova, I., Mews, A., and Basch, T. 2003. Scanning near-field optical microscopy using semiconductor nanocrystals as a local fluorescence and fluorescence resonance energy transfer source. J. Microsc. **210**: 274–278.
23) Steyer, J.A., and Almers, W. 2001. A real-time view of life within 100 nm of the plasma membrane. Nat. Rev. Mol. Cell Biol. **2**: 268–275.
24) Toomre, D., and Manstein, D.J. 2001. Lighting up the cell surface with evanescent wave microscopy. Trends Cell Biol. **11**: 298–303.
25) Voura, E.B., Jaiswal, J.K., Mattoussi, H., and Simon, S.M. 2004. Tracking metastatic tumor cell extravasation with quantum dot nanocrystals and fluorescence emission-scanning microscopy. Nat. Med. **10**: 993–998.
26) Wiese, R., Belosludtsev, Y., Powdrill, T., Thompson, P., and Hogan, M. 2001. Simultaneous multianalyte ELISA performed on a microarray platform. Clin. Chem. **47**: 1451.
27) Wu, X., Liu, H., Liu, J., Haley, K.N., Treadway, J.A., Larson, J.P., Ge, N., Peale, F., and Bruchez, M.P. 2003.

Immunofluorescent labeling of cancer marker Her2 and other cellular targets with semiconductor quantum dots. Nat. Biotechnol. **21**: 41–46.

28) Xu, H., Sha, M.Y., Wong, E.Y., Uphoff, J., Xu, Y., Treadway, J.A., Truong, A., O'Brien, E., Asquith, S., Stubbins, M., Spurr, N.K., Lai, E.H., and Mahoney, W. 2003. Multiplexed SNP genotyping using the Qbead system: a quantum dot-encoded microsphere-based assay. Nucleic Acids Res. **31**: 43.

29) Zhao, X., Hilliard, L.R., Mechery, S.J., Wang, Y., Bagwe, R.P., Jin, S., and Tan, W. 2004. A rapid bioassay for single bacterial cell quantitation using bioconjugated nanoparticles. Proc. Natl. Acad. Sci. U.S.A. **101**: 15027–15032.

Imaging Agents

Water-Soluble Photoluminescent Silicon Quantum Dots**

*Jamie H. Warner, Akiyoshi Hoshino, Kenji Yamamoto, and Richard. D. Tilley**

The quantum confinement of excitons in semiconductor quantum dots leads to interesting optical properties that can be exploited in a range of photonic applications including biological fluorescence imaging[1–6] and optoelectronic devices.[7–13] Quantum dots are becoming popular as replacements for fluorescent dyes in biological fluorescence imaging because of their superior stability against photobleaching. To date, considerable emphasis has been placed on using CdSe quantum dots with a ZnS shell as biological chromophores since they emit light that can be tuned throughout the visible spectrum.[14] However, concerns have been raised about the toxicological issue of using cadmium in biological systems.[15] In particular, Derfus et al. showed that CdSe quantum dots without a ZnS shell were toxic to liver cells after exposure to UV light.[15] The potential biocompatibility of silicon makes photoluminescent silicon quantum dots an ideal candidate for biological fluorescence imaging and should eliminate any potential toxicology problems that might arise from having a CdSe core.[16,17]

Strong quantum confinement in silicon increases the probability of radiative recombination through the direct band gap transitions and reduces phonon-assisted indirect band gap transitions.[18] In silicon, this requires the physical dimensions of the quantum dots to be on the order of or less than the bulk exciton Bohr radius of 4 nm.[19,20] Quantum dot sizes of less than 8 nm are easily achieved using wet chemistry techniques.[19–22] The remarkably successful advances in the synthesis of the semiconductor groups II/VI and III/V have not been applied to silicon as a consequence of the relatively high temperatures required to degrade the precursor and to produce highly crystalline quantum dots. The greatest success in producing silicon quantum dots with strong quantum confinement to date has been by the solution-phase reduction of silicon salts.[19,21,22]

[*] J. H. Warner, R. D. Tilley
School of Chemical and Physical Sciences
MacDiarmid Institute of Advanced Materials and Nanotechnology
Victoria University of Wellington
P.O. Box 600, Wellington (New Zealand)
Fax: (+64) 4-463-5237
E-mail: richard.tilley@vuw.ac.nz
A. Hoshino, K. Yamamoto
Department of Medical Ecology and Informatics
Research Institute
International Medical Center of Japan
Toyama 1-21-1, Shinjuku, Tokyo 162-8655 (Japan)

[**] J.W. and R.D.T. thank the MacDiarmid Institute of Advanced Materials and Nanotechnology for funding. J.W. and R.D.T. thank H. Rubinsztein-Dunlop for the use of the time-resolved PL spectroscopy system at The University of Queensland.

The solution-phase synthesis of silicon quantum dots has previously been reported by Kauzlarich and co-workers[21,22] through the use of a variety of reducing agents, by Korgel and co-workers[19,23] through the use of high temperatures and pressures, and by Wilcoxon et al. by using micelles.[20,24] The current problem associated with the simpler room-temperature syntheses [20–22] is the large size distribution produced. The large size distribution prevents a simple interpretation of the optical spectra. Post-synthesis treatments for narrowing the size distribution of the silicon quantum dots, such as high-pressure gas chromatography (HPGC), have revealed sharp features in the absorption spectra and narrow photoluminescence spectra attributed to direct band gap transitions.[20] We have recently reported the synthesis of 1–2-nm silicon quantum dots that were surface-passivated by 1-heptene. These dots had a narrower size distribution than previously reported and gave a strong blue photoluminescence.[25]

For silicon quantum dots to be used in biomedical applications it is essential that they have a substantial photoluminescence quantum yield in the visible region, have a fast radiative recombination rate, and are water soluble and hydrophilic to prevent aggregation and precipitation in a biological environment. The chemical process used to terminate the surfaces of the silicon quantum dots changes the internal electronic structure and thus plays an important role in the resultant emission wavelength and radiative lifetime, and ultimately determines the solubility.[18] Silicon quantum dots with an oxide surface passivation typically display a dipole-forbidden yellow-red emission with radiative lifetimes of 10^{-3}–10^{-6} s.[18,26] This slow rate of recombination limits the use of oxide-passivated silicon quantum dots in biological imaging. However, silicon quantum dots with a hydrogen or carbon surface passivation have electric-dipole-allowed direct band gap transitions that lead to blue photoluminescence with fast recombination rates of 10^{-8}–10^{-9} s.[18,20]

In this study we describe a simple room-temperature synthesis for producing water-soluble silicon quantum dots that exhibit strong blue photoluminescence with a rapid rate of recombination. The use of hydride reducing agents in these experiments produce hydrogen-terminated particle surfaces.[20,24,25] The Si–H surface bond can then be treated with both a compound containing a C=C bond and a platinum catalyst to produce a variety of surface types through formation of a Si–C surface bond. The surface of the silicon quantum dots are modified with allylamine to form hydrophilic silicon quantum dots (Figure 1). Previous reports of changing the surface-capping molecules of silicon particles have involved treating chloride-terminated particle surfaces with Grignard reagents to produce particles capped with organic molecules[27] or utilized a Si–OR bond.[22] Silicon quantum dots with a chlorine-terminated surface are restricted to a small range of available Grignard reagents, whilst Si–OR bonds have been shown to greatly affect the electronic charge distribution in the silicon quantum dots and consequently reduce the energy of indirect transitions.[18,26]

Figure 2 shows a high-resolution transmission electron microscope (HRTEM) image of a number of allylamine-capped silicon quantum dots on a carbon-coated copper grid.

  DOI: 10.1002/anie.200501256

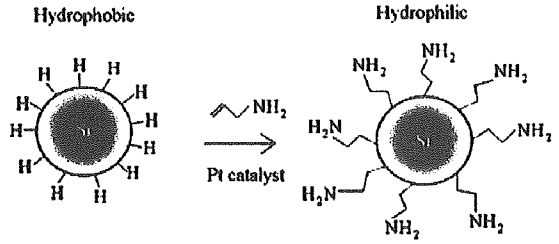

Figure 1. Schematic diagram of the procedure used to change the surface chemistry of the silicon quantum dots from hydrogen to allylamine.

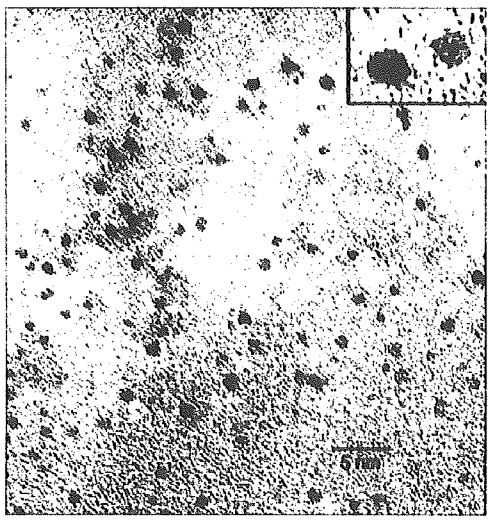

Figure 2. High-resolution transmission electron microscopy (HRTEM) image of a large number of allylamine-capped silicon quantum dots. Inset: HRTEM image of two silicon quantum dots showing the crystal lattice planes.

The water-soluble silicon quantum dots were highly crystalline and the atomic lattice planes of two separate silicon quantum dots can be clearly seen in the inset of Figure 2. Fast Fourier transform (FFT) analysis of the crystal structure shown in the inset of Figure 2 could be matched with the (2,1,−1) and (2,−1,1) planes of diamond silicon when viewed down the [011] direction. The low atomic weight of silicon relative to other metallic and semiconductor quantum dots combined with their extremely small dimensions resulted in low contrast in the HRTEM images. Only by removing almost all of the surfactant (TOAB) could such small (1–2 nm) silicon quantum dots be imaged by HRTEM. Figure 2 shows a relatively high contrast HRTEM image of the 1–2-nm silicon quantum dots along with minimal surfactant, thus indicating that a high level of purification had been achieved. The high purity of the silicon quantum dots enables the photoluminescence to be assigned to the quantum dots and not to other by-products of the reaction, such as silicon-based organosilane polymer/oligomers.

The small dimensions of the silicon quantum dots limits the selected-area electron-diffraction and X-ray diffraction measurements, and no conclusive results have as yet been obtained by using these techniques. The silicon quantum dots were also faceted, which reflects the controlled growth environment.[19] A mean size and size distribution of 1.4 ± 0.3 nm of the allylamine-capped silicon quantum dots was obtained by analyzing 648 quantum dots from different regions on the TEM grid. This small size distribution is a significant improvement on previous reports of 1–2-nm silicon quantum dots synthesized in inverse micelles.[20–22] Energy-dispersive X-ray spectroscopy (EDS) performed on the quantum dots showed a strong peak associated with silicon and no peaks for platinum. This observation confirmed that the platinum catalyst had successfully been removed during purification.

The bonding of allylamine to the surface of the silicon quantum dots was confirmed by FTIR spectroscopy (Figure 3). Peaks were observed at 1460 and 1260 cm^{-1} and

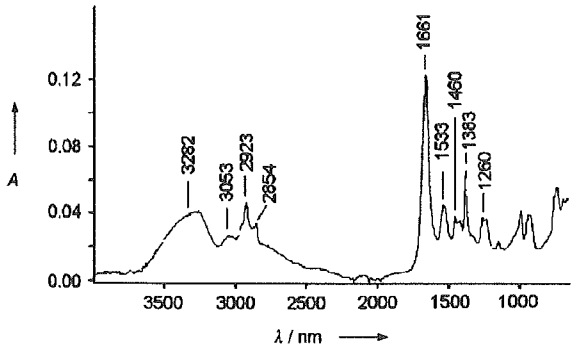

Figure 3. FTIR spectrum of allylamine-capped silicon quantum dots.

attributed to the vibrational scissoring and symmetric bending of $Si–CH_2$.[27] The absorbance between 2500 and 3500 cm^{-1} is attributed to symmetric and asymmetric vibrations of the $C–CH_2$ and $C–NH_3$ molecular components of the allylamine, while the dominant peak at 1661 cm^{-1} is attributed to the allylamine and clearly indicates its attachment to the silicon quantum dots. The peaks between 1000 and 1100 cm^{-1} are attributed to the vibrational stretching of Si–OR.[21] Despite the fact that the silicon quantum dots were heated in atmospheric conditions to remove the solvent for FTIR measurements, the magnitude of the Si–OR vibration is very small when compared to the FTIR reports of siloxane-coated silicon quantum dots, which have a total Si–OR surface coverage.[21] This difference highlights the strength and stability of the Si–C bond formed between the silicon quantum dots and the allylamine as well as the minimal number of Si–OR surface bonds present.

The absorption spectrum of the allylamine-capped silicon quantum dots in water (Figure 4a, curve I) displays a feature at 320 nm which is attributed to the Γ-Γ direct band gap transition.[19,20] This direct band gap transition has blue-shifted because of the effect of quantum confinement in the quantum dots—from the bulk value of 3.4 to 3.8 eV in these silicon quantum dots—and is in good agreement with other reports.[19,20]

The photoluminescence (PL) spectra recorded at 300 and 400 nm (Figures 4a, curves II and III) show a peak at 480 nm

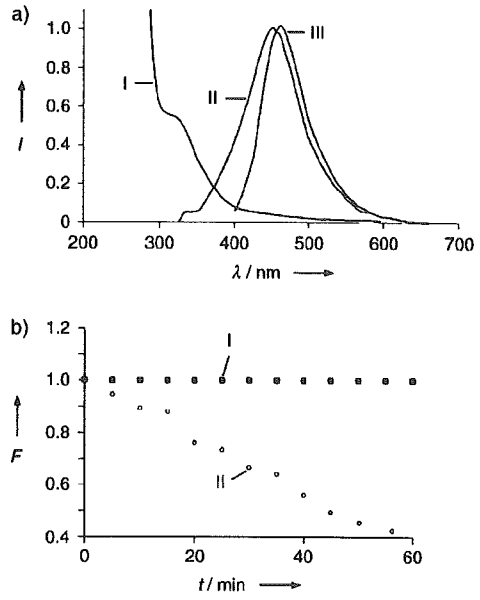

Figure 4. a) Curve I: Absorption spectrum of allylamine-capped silicon quantum dots in water; curve II: photoluminescence spectrum of allylamine-capped silicon quantum dots in water with excitation at 300 nm; curve III: photoluminescence spectrum of allylamine-capped silicon quantum dots in water with excitation at 400 nm. b) Integrated photoluminescence as a function of time of allylamine-capped silicon quantum dots in water (curve I) and rhodamine 6G in water (curve II). An excitation wavelength of 400 nm was used in both cases.

with a full-width at half maximum height (FWHM) of 70–80 nm. All the spectra in Figure 4 have been scaled for clarity of presentation.

Photoluminescence quantum yields of the allylamine-capped silicon quantum dots in water were obtained by using the comparative method of Williams et al.[28] PL quantum yields of up to 10% were obtained relative to the standard, 9,10-diphenylanthracene, in cyclohexane.[29] The optical properties of the colloidal solutions of the allylamine-capped silicon quantum dots were stable for several months. The silicon quantum dots showed better photobleaching stability than the fluorescent dye, rhodamine 6G in water, on excitation with UV light (Figure 4b). The silicon quantum dots showed no signs of any measurable photobleaching (Figure 4b, curve I) under the same illumination conditions during which the photoluminescence from rhodamine 6G dropped by 60% (Figure 4b, curve II).

The origin of the photoluminescence observed in Figure 4 is complicated by the combination of both indirect and direct band gap transitions present in silicon quantum dots and is actively debated.[19] However, there is strong theoretical evidence suggesting that 1–2-nm silicon quantum dots with a hydrogen or carbon surface termination have direct band gap optical transitions that lead to photoluminescence in the UV/blue region of the electronic spectrum.[18] The emission observed in Figure 4a is consistent with the theoretical predictions of direct band gap recombination in silicon quantum dots with carbon surface termination rather than from trap states or surface states, or of silicon quantum dots with oxygen surface termination. Emission from a Si–OR-terminated silicon quantum dot is typified by an emission centered at 600 nm.[20,30]

Further insights into the nature of the photoluminescence can be obtained by analyzing the time-resolved photoluminescence spectra from the allylamine-capped silicon quantum dots in water. Figure 5 shows the time-resolved photoluminescence decays from an aqueous solution of allylamine-capped silicon quantum dots at two different emission wavelengths. The PL decay measured at 420 nm (Figure 5, curve a) is noticeably shorter than the PL decay measured at 500 nm in curve b. Both PL decays required a three exponential fit with an overall average decay of 4 ns.

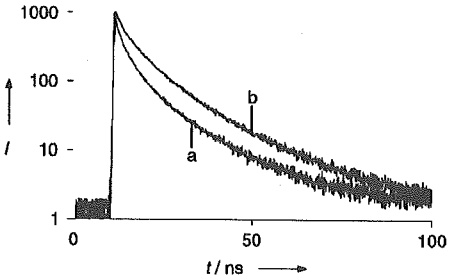

Figure 5. Time-resolved photoluminescence decays of allylamine-capped silicon quantum dots in water measured at emission wavelengths a) 420 nm and b) 500 nm. An excitation wavelength of 380 nm was used.

Indirect band gap materials, such as silicon, generally have slow recombination with PL lifetimes on the order of tens of microseconds to milliseconds, whereas direct band gap materials, such as GaAs and CdSe, have fast recombination with PL lifetimes on the order of 1–10 ns.[31] The PL lifetime measurements obtained here are in good agreement with the experimental findings of the research groups of Korgel [23] and Wilcoxon[20] as well as the theoretical predictions of Zhou et al.[18] The rapid rates of recombination measured here provide strong evidence that the observed emission results from dipole-allowed recombination across the direct band gap transition in silicon quantum dots with a carbon surface termination.

The suitability of allylamine-capped silicon quantum dots as a chromophore for biological imaging is demonstrated in Figure 6, for which an excitation wavelength of 365 nm was used and the emission at 480 nm was monitored. The control image (Figure 6a) shows minimal fluorescence from the HeLa cells relative to the HeLa cells with the incorporated silicon quantum dots (Figure 6b). Thus, the fluorescence observed in the HeLa cells in Figure 6b arises from the emission from silicon quantum dots and not autofluorescence from the cells. The inset in the top left corner of Figure 6b shows the bright blue fluorescence from a vial of allylamine-capped silicon quantum dots in water when excited with UV light. The bright blue fluorescence from the silicon quantum dots is distributed uniformly inside the cytosol of the HeLa cells and this shows the possibility of using these hydrophilic silicon quantum dots as chromophores in biological fluores-

